Ab initio and finite-temperature molecular dynamics studies of lattice resistance in tantalum

D. E. Segall*
Department of Physics, Massachusetts Institute of Technology, Cambridge, Massachusetts 02139, USA

Alejandro Strachan† and William A. Goddard III
Materials and Process Simulation Center, Beckman Institute (139-74), California Institute of Technology, Pasadena, California 91125, USA

Sohrab Ismail-Beigi
Department of Physics, University of California at Berkeley, Berkeley, California 94720, USA

T. A. Arias
Laboratory of Atomic and Solid State Physics, Cornell University, Ithaca, New York 14853, USA
(Received 6 December 2002; revised manuscript received 21 April 2003; published 10 July 2003)

We explore the apparent discrepancy between experimental data and theoretical calculations of the lattice resistance of bcc tantalum. We present an empirical potential calculation for the temperature dependence of the Peierls stress in this system and an *ab initio* calculation of the zero-temperature Peierls stress, which employs periodic boundary conditions, those best suited to the study of metallic systems at the electronic-structure level. Our *ab initio* value for the Peierls stress is over five times larger than current extrapolations of experimental lattice resistance to zero temperature. Although we find that the common techniques for such extrapolation indeed tend to underestimate the zero-temperature limit, the amount of the underestimation we observe is only 10%-20%, leaving open the possibility that mechanisms other than the lattice resistance to motion of an isolated, straight dislocation are important in controlling the process of low-temperature slip.

DOI: 10.1103/PhysRevB.68.014104 PACS number(s): 62.20.Fe, 71.15.Mb, 71.15.Pd

I. INTRODUCTION

The study of the plasticity of crystalline materials is a rich many-body problem involving physics on multiple length scales, with many remaining unexplained mysteries. The plasticity of bcc metals, for instance, is particularly challenging. Unlike their fcc and hcp counterparts, the bcc metals exhibit many active slip planes, have a strong temperature dependence in their plasticity, and violate the simple empirical Schmid law.[1,2] Moreover, theoretical calculations of the most basic question in plasticity, the stress needed to induce yield at low temperature in a pure sample, differ from experimental extrapolations by over a factor of 2.[1] The purpose of this work is to provide needed insight into this discrepancy.

It is generally believed that it is the physics of the $\langle 111 \rangle$ screw dislocation defect which controls the low-temperature plasticity of bcc materials.[1,2] The Peierls stress, the yield stress at which these dislocations first begin to move spontaneously, is difficult to compare directly with experiment. Whereas most computational work on the Peierls stress measures the stress to move an isolated, infinitely straight dislocation at zero temperature,[2–14] experiments measure the Peierls stress at a finite temperature in systems with many interacting, curved dislocations and in media with defects and surfaces. As an example of the present challenges, using model generalized pseudopotential theory (MGPT),[12] Yang *et al.*[9] predicted for the $T=0$ Peierls stress a value 2.5 times greater than experimental extrapolations.[15] Because such potentials are not based upon first principles, it is impossible to determine *a priori* whether this discrepancy is due to the interatomic potential, the environmental complexities discussed above, or to a flaw in our understanding of the relation between the Peierls stress and the experiments.

Since it is a daunting experimental task[16] to observe properties of a single dislocation locked deep in the heart of a material, accurate theoretical calculations of such systems are essential. Nearly all theoretical calculations to date, concerning such dislocations, have relied upon empirical potentials.[2–6,9–14,17,18] Given the empirical nature of such calculations, the complex directional bonding properties of bcc materials, and the lack of direct comparison with experiments for validation, first-principles *ab initio* calculations of dislocations in such systems are clearly needed. Ismail-Beigi and Arias[19] showed that density-functional theory calculations were crucial for understanding the fundamental properties of the $\langle 111 \rangle$ screw dislocation core structure in bcc molybdenum and tantalum. Until that work, most computational studies based on empirical potentials[2–6,10–12] supported the idea that the dislocation core breaks symmetry, with two energetically equivalent ground-state structures which spread outward along two different equivalent sets of three {110} planes,[2] similar to the concept originally proposed by Hirsch and co-workers.[2,20] Until the availability of the *ab initio* calculations, the prevailing view of the violation of the Schmid law in the bcc metals was based upon this structure.[2] Ismail-Beigi and Arias,[19] in contrast, showed that for both molybdenum and tantalum the ground-state structure within density-functional theory was a nondegenerate symmetric core, supporting the work of Suzuki, Takeuchi,

and co-workers[13,21,22] which first suggested that it is the Peierls potential itself that controls the lattice resistance and not the details of the core structure. To help resolve the discrepancy between theoretical and experimental Peierls stresses, the work below provides a reliable *ab initio* prediction of the Peierls stress in bcc tantalum which is free of the unrealistic electronic boundary conditions employed in the only other *ab initio* prediction of the Peierls stress.[7,8]

Here, we show that the Peierls stress, calculated within density-functional theory, is over a factor-of-5 larger than expected from extrapolation of experimental results.[15] This supports the view that the discrepancy between the experimental and computational predictions is largely due to the aforementioned environmental complexities, to a flaw in relating the experimental data to the Peierls stress, or to a combination of both.

To further explore possible physical effects leading to this discrepancy, we study the extrapolation of experimental data to determine the zero-temperature Peierls stress. Such extrapolations generally employ fits from mesoscopic or thermodynamics/kinetic models.[15,23–25] However, it has not been established that such models can accurately describe the lowest-temperature regime correctly, placing doubt on the quality of these extrapolations. To address this issue, the work below also provides a temperature- and orientation-dependent study of the Peierls stress, in which empirical potentials are employed. We moreover show that extrapolation of our finite-temperature results using a current fitting model leads to an underestimation of the zero-temperature Peierls stress. This underscores the difficulty in extrapolating the experimental data accurately but does not fully account for the observed discrepancy.

In Sec. II, we review the various techniques in use for calculation of the Peierls stress in the context of efficacy for application to *ab initio* calculations. Section III gives the calculation of the temperature- and orientation-dependent Peierls stress in a bcc material. Section IV describes our technique for obtaining Peierls stresses within small unit cells with periodic boundary conditions. Finally, Sec. V presents our *ab initio* prediction for the Peierls stress and compares and contrasts it to currently available experimental and computational values.

II. BOUNDARY CONDITIONS

The fundamental distinction among theoretical approaches to calculation of the Peierls stress is the choice of boundary condition. The literature describes three types of boundary conditions: cylindrical boundary conditions,[2–4,10,12–14,17] Greens-function (or ''flexible'') boundary conditions,[2,6–9,26,27] and periodic boundary conditions.[4,5,18] We now briefly review each with emphasis on the unique challenges of *ab initio* electronic-structure calculations.

A. Cylindrical boundary conditions

In the practice of cylindrical boundary conditions, anisotropic elasticity theory[28–30] is used to generate a dislocation in the center of a cylinder. The cylinder is then separated into *inner* and *outer* regions. The atoms in the outer region are held fixed to the solution of anisotropic elasticity theory while the atoms in the inner region relax under the interatomic forces. To calculate the Peierls stress, a stress is applied to the system until the dislocation moves.

This approach suffers numerous drawbacks when applied to density- functional theory. To avoid surface effects and to properly account for the nonlinear nature of the dislocation, such cylinders generally have to be quite large. First, even the outer cylinder is of finite size and therefore the outer region must be sufficiently large enough so that forces it generates onto the inner region are equivalent to those generated from an infinite continuum. The inner region also must be sufficiently large to mitigate two effects. The inner region must be large enough so that linear elasticity theory represents well the forces it imposes on the outer region. The inner region also must be large enough so that motion of the dislocation is not adversely affected by the fixed outer region, which is a concern because the fixed outer region represents the displacement field when a dislocation is at its center and therefore generates a extraneous force that tends to prevent motion of the dislocation.[17] When using simple, interatomic potentials, the use of large cylinders mitigates all of these effects. However, this approach is not viable for density-functional calculations with their extreme computational demands.

This approach, moreover, is particularly ill suited for electronic-structure calculations because the artificial surface at the outside of the outer region, being quite different from the bulk, give rise to strong scattering of the electrons very different than that of an infinite continuum. This is particularly problematic for metals, because the single-particle density matrix, which quantifies the effects of this scattering on the interatomic forces, decays only algebraically in metals.[31] The following section demonstrates that the boundary regions should be quite large in order to prevent these surface effects from resulting in large fictitious forces in the active region of the calculation.

B. Greens-function boundary conditions

The use of Greens-function, or flexible, boundary conditions[2,26,27] is an effective way to reduce the size of the simulation cell. This approach also employs a cylindrical geometry. However, rather than the ''inner'' and ''outer'' atomistic regions of the cylindrical boundary approach, the Greens-function approach employs three interatomic regions: an inner- ''core'' region containing the center of the dislocation, an intermediate ''buffer'' region, and an outermost ''continuum-response'' region. With *proper* implementation, the outer and inner regions couple only indirectly through the response of the buffer region.

In this method, all three regions respond to the presence of a dislocation; however, the response of each region is treated differently through a number of steps. Initially, all regions are displaced by the solution to anisotropic elasticity theory. Each iteration then begins by relaxing the atoms in the core region according to the forces which they experience, as computed from either an interatomic potential or an *ab initio* method. The forces generated from the mismatch

between the outer and inner regions, which the cylindrical approach above ignores, are then relieved by moving the atoms of *all three regions* according to the elastic Greens-function solution, leaving only the nonlinear effects from the core region unaccounted. The next iteration then begins by relaxing these forces as described above. Iterations proceed until until the forces in the core and buffer regions are negligible.

What distinguishes this approach from simple cylindrical boundary conditions is that the continuum region, via the Greens-function response, is allowed to respond to the motion of the dislocation and to the elastic response generated by the core region as the dislocation moves. So long as the continuum-response region (i) accurately represents the structure induced by the presence of the dislocation and (ii) is sufficiently wide to properly reproduce the forces on the atoms in the buffer and inner regions, this approach accurately describes basic properties of a dislocation.

In order for the first assumption (i) above to hold, the inner-core region must be sufficiently large to contain all atoms with displacements outside of the linear regime and the buffer region must be sufficiently wide so that displaced atoms in the core have no direct effect on the forces experienced in the continuum-response region. The second assumption (ii) requires that the continuum-response region be sufficiently large so that its termination has no effect on the forces on the atoms in the buffer or inner region. The radius of the calculation must therefore exceed the sum of the nonlinear core radius plus twice the range over which motion of atoms creates forces within the lattice. Since the latter range can be quite large for electronic-structure calculations in metals, the application of this approach to electronic-structure calculations can be problematic.

The Greens-function approach has predicted successfully dislocation properties when applied to time-consuming empirical potentials[6,9] which have a limited interaction range. The approach also has been applied to density-functional calculations of the Peierls stress for molybdenum and tantalum,[7,8] where its application is more questionable due to the above interactions. In these latter works, the artificial boundary on the outside of the continuum-response region has been treated in one of two ways,[7,8] either by keeping the surface free in vacuum or by embedding in periodic boundary conditions with the vacuum filled with material which must contain severe domain boundaries due to the incompatibility of a net Burgers vector with periodic boundary conditions. To gauge the effects this artificial boundary may have and how far these effects penetrate from the continuum-response region into the buffer region, we perform a test calculation within the density-functional theory pseudopotential approach[32] of the magnitude of the forces generated onto the system due to the presence of a domain boundary similar to those in the works cited above.[7,8]

For this calculation, we employ the same computational procedure as for our production calculations in Sec. V. Here, however, since this is a test, we employ only a single k point to sample the Brillouin zone (Γ). We begin with an orthorhombic cell of 24 atoms of tantalum in a bulk arrangement with supercell lattice vectors $\vec{r}_1 = a[1\bar{1}0]$, $\vec{r}_2 = 4a[11\bar{2}]$, and $\vec{r}_3 = a/2[111]$, where a is the lattice constant of the cubic unit cell. We choose this cell because its length along $\vec{r}_2$ is the same as the smallest simulation cell used in Refs. 7 and 8. We then generate a domain boundary at the edge of cell along the $(11\bar{2})$ plane by changing the lattice vector $\vec{r}_2$ to $\vec{r}_2 = 4a[11\bar{2}] + \alpha\vec{r}_3$ and holding the atoms in the unit cell fixed in their bulk locations. α is chosen such that the shift is small and the nearest neighbor distance is always within 95% of the bulk, representing even less of a disturbance than that in Ref. 7, where atoms were within 90% of the bulk nearest-neighbor distance. To estimate the effect of the scattering of electrons at the domain boundary on the interatomic forces, we hold the atoms fixed and compute the *ab initio* forces acting upon them.

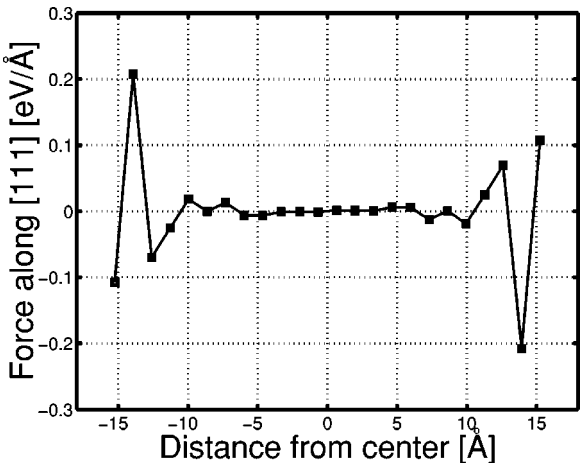

FIG. 1. Force on the atoms, along the [111], due to the presence of a domain boundary. The forces are plotted as a function of distance from the center of the unit cell. The domain boundary is generated such that the nearest-neighbor distance is always within 95% of the bulk ($\alpha = 1/4$).

Figure 1 shows the forces along the [111] direction as a function of distance from the center of each domain. Note that relatively large forces develop deep within the cell. This data indicates that the continuum-response region should be quite large ($\approx 5-10$ Å) in order to prevent the response of the electrons from adversely effecting the forces in the buffer region. Note also that the buffer region should be of similar width to prevent forces from the nonlinear displacements in the core from penetrating into the linear continuum-response region. Such large continuum-response and buffer regions can make the calculation incompatible with current computational techniques.

In fact, the only density-functional calculations of the Peierls stress in this system to date employ the Greens-function method but with a distance from the buffer region to the domain boundary of only ≈ 3.7 Å . It thus is unclear whether the continuum region in these calculations is sufficiently large enough to yield reliable results and clearly further calculations are needed to support those results. Below, we provide just such calculations using the method of periodic boundary conditions, which perturb the electronic system far less than the introduction of domain boundaries.

C. Periodic boundary conditions

The final common choice for boundary conditions is to repeat the dislocation core periodically throughout space, so that the dislocation is no longer isolated, but embedded in bulk material containing an array of dislocations. Consistency with periodic boundary conditions then demands that the unit cell contain a net zero Burgers vectors, arranged typically in a dipolar[33–35] or quadrupolar[19,35,36] array. For static properties of the dislocation core, such cells give reliable results as the elastic fields of the surrounding dislocations effectively cancel at the location of each core.

Periodic boundary conditions can also be used to calculate the Peierls stress.[4,5,18] Care must be taken, however, because the material properties of a densely packed array of dislocations can be quite different from those of bulk. The use of large unit cells can control this effect;[18] however, such a direct, brute-force approach is not practical for computationally demanding *ab initio* calculations. To make such calculations feasible, they must occur in small periodic cells, thereby demanding proper accounting for the presence of many neighboring dislocations.

We have shown in another work[4] that, under certain conditions, such effects can be accounted for accurately with minimal extra computational effort, so that accurate values of the Peierls stress can be obtained from density-functional calculations in periodic cells. Since the residual errors with this approach are associated with the boundary conditions, the magnitude of such an error can be tested by using other computational methods, such as empirical potentials. Our previous work shows that this residual error is relatively small,[4] a fact which we confirm explicitly below.

Because the deviations from the bulk arrangement at periodic boundaries are relatively mild, such calculations are ideal for mitigating electronic boundary effects. Given the simplicity of working with these boundary conditions and the possibility of the extraction of accurate values for the Peierls stress from small unit cells, we choose to work with periodic boundary conditions throughout this work. Section IV outlines our procedure for calculating the Peierls stress while working with periodic boundary conditions and describes the sources and the magnitude of the residual errors. (See Ref. 4 for a full discussion of these issues.)

III. DEPENDENCE OF THE PEIERLS STRESS ON ORIENTATION AND TEMPERATURE

To illustrate the complexities of relating computational predictions to experimental findings, we now explore the dependence of the Peierls stress in bcc tantalum on orientation and temperature. The strong dependencies that we find underscore the unique properties of dislocations in bcc metals. To clarify, since some authors use slightly different definitions for the Peierls stress, here we consider the Peierls stress as the value of the stress on the maximum resolved shear stress plane (maximum value of the shear stress along the [111] direction) when the dislocation *first* moves to a different equilibrium position.

Despite recent advances in *ab initio* quantum-mechanical methods, such methods are still too computationally intensive to study such properties as the temperature dependence of the Peierls stress. Therefore, for these calculations, we employ a molecular-dynamics (MD) framework carried out using a first-principles-based embedded atom method (qEAM), many-body force field (FF) for tantalum which we have developed to allow accurate and computationally efficient evaluation of atomic interactions.[5,37]

TABLE I. Peierls stress for the $\langle 111 \rangle$ screw dislocation in tantalum in the twinning, $\langle 112 \rangle$, and antitwinning directions; the last column shows the ratio between antitwinning and twinning Peierls stresses. MGPT results are from Yang *et al.* (Ref. 9).

Potential	Twin	$\langle 112 \rangle$	Antitwin	Asymmetry
qEAM FF	575 MPa	655 MPa	1075 MPa	1.6412
MGPT	605 MPa	640 MPa	1400 MPa	2.29

As described above, we carry out these calculations within periodic boundary conditions. The supercell consists of a quadrupolar arrangement[35,36] of dislocations containing 5670 atoms with lattice parameters $a_x = 70.59$ Å, $a_y = 73.39$ Å , and $a_z = 20.11$ Å , where the x, y, and z axes of our coordinate system are along $[1\bar{1}0]$, $[11\bar{2}]$, and $[111]$ directions, respectively. As we have shown in another work,[4] such a cell gives very accurate values for the Peierls stress.

A. Orientation dependence of the zero-temperature Peierls stress of the $\langle 111 \rangle$ screw dislocation

To calculate the zero-temperature Peierls stress, we start with a fully relaxed quadrupole dislocation configuration at zero stress and increase the stress in steps of 50 MPa until the dislocations move. Once the dislocations move, we restart the calculation from the structure equilibrated just prior to the motion and increase the stress in smaller steps (5 MPa) in order to more narrowly define the critical stress. At each incremental target stress, we relax the atoms and stresses in the cell by running two very low-temperature ($T = 0.001$ K) MD simulations. The first run is for 15 ps at constant stress and temperature ($N\sigma T$ ensemble) using a Parinello-Rahman barostat[38] and a Hoover[39] thermostat, and the second run is for 50 ps at constant volume and temperature (NvT ensemble). We find this approach to be quite stable for relaxing the cell and the atoms of the system.

The $\langle 111 \rangle$ screw dislocation has three equivalent {112} and three equivalent {110} potential slip planes, with such planes occurring at 30° intervals. To study the orientation dependence of the Peierls stress, we apply three types of pure shear stress to the system: a σ_{xz} stress, a positive σ_{yz} stress, and a negative σ_{yz} stress. (Note that with coordinate axes as defined above, the z axis lies along the dislocation line.) These stresses lead to forces on the dislocation in the $\langle 112 \rangle$, $\langle 110 \rangle$-twinning, and $\langle 110 \rangle$-antitwinning directions, respectively.[28] Along these directions, we find Peierls stresses of $\tau_{112} = 655$ MPa, $\tau_{twin} = 575$ MPa, and $\tau_{anti} = 1075$ MPa, respectively. Table I shows that our essentially zero-temperature results are in good agreement with those of Yang and collaborators,[9] who employed model generalized

pseudopotential theory (MGPT),[12] a different interatomic potential. The result of such a strong dependence of the Peierls stress on orientation is consistent with the experimentally observed breakdown of the Schmid law in bcc metals.

To make quantitative comparison with experiments, which were carried out at nonzero temperature, we compare our results to those of Tang *et al.*,[15] who fitted experimental data[40] to a mesoscopic model and then extrapolated to extract the zero-temperature Peierls stress. Their predicted value of 248 MPa for the $\langle 112 \rangle$ Peierls stress is over a factor-of-2 lower than our result. This type of discrepancy, where the theoretical Peierls stress overestimates the zero-temperature extrapolation of the experimental data by a factor of 2 to 3, is quite generally observed.[1] This discrepancy may be due either to inaccuracies in the theoretical calculations or, perhaps, a flaw in the comparison between the zero-temperature extrapolation of the experimental data and theoretical predictions.

B. Temperature dependence of the Peierls stress of the $\langle 111 \rangle$ screw dislocation

To explore potential difficulties with the zero-temperature extrapolation, we now present what is to our knowledge the first temperature-dependent study of Peierls stress using a realistic potential for a bcc metal. For these calculations, we continue to employ the qEAM FF and begin with the zero-temperature, equilibrated structures. We then apply various constant shear stresses (lower than the $T=0$ Peierls stress) to the system while slowly increasing the temperature (in steps of 10 K) until the dislocations move. Similarly to the $T=0.001$ K case, for each temperature we first run for 10 ps in the $N\sigma T$ ensemble and then for 25 ps in NvT ensemble.

Because the Peierls stress can depend on the rate at which the strain is applied, to place our results in context, we first estimate the strain rate in our computations. The strain rate is approximately $\dot{\gamma}=\rho v_d b$, where v_d is the dislocation velocity, ρ is the dislocation density, and b is the Burgers vector. Using a dislocation density typical of the experiments[15] ($\rho = 10^{11}\times 1/\mathrm{m}^2$)and estimating the dislocation velocity as the ratio between the distance traveled in one jump ($1/3a\langle 112 \rangle = 2.717$ Å) and the simulation time (35 ps), we obtain an effective strain rate of $\sim 10^2 \times 1/\mathrm{s}$, which is large compared to the strain rates (4×10^{-5}) in the experiments used for the zero-temperature extrapolations.[15,40]

Figure 2 summarizes our results for the temperature dependence of the Peierls stress as a function of temperature for the three directions ($\langle 112 \rangle$, twinning, and antitwinning). As expected, the Peierls stress obtained from our MD simulations decreases rapidly with increasing temperature, particularly for very low temperatures. It is important to mention that, although our simulations are three dimensional, the dislocations move as straight lines without the formation of double kinks because our simulation cell is only seven Burgers vectors long along the dislocation lines. Such double kinks are quite important at finite temperatures since they tend to lower the lattice resistance at nonzero temperatures. Our results are approximately a factor-of-2 to 4 larger than the fit of Tang *et al.*[15] to the experimental data of

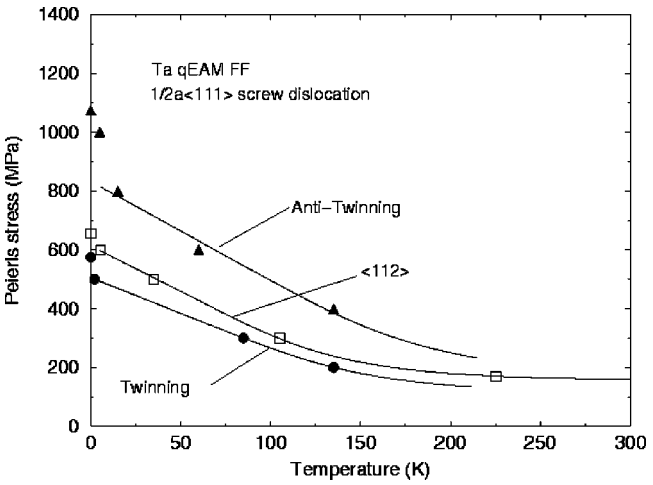

FIG. 2. Temperature dependence of the Peierls stress along various directions: the $\langle 112 \rangle$, twinning and antitwinning directions. The fits are done for the high-temperature data using Eq. (1). The temperature is in degrees Kelvin, and the stress in mega-Pascals.

Wasserbach.[40] We feel that this is reasonable, considering the facts that our simulation cells do not allow for double kink formation and that, as discussed above, our strain rates are much higher than those in the experiments.[15,40]

Experimental extrapolations of the Peierls stress to zero temperature generally come from mesoscopic or kinetic/thermodynamic model[15,23–25] fits to experimental data and are then extrapolated to zero temperature. To explore the effects of this procedure, we fit our atomistic data to such a model, perform the extrapolation, and then compare with our direct zero-temperature results.

For the fit we use an analytical expression for the dependence of the Peierls stress with temperature at constant strain rate[24,25] based on a mechanism involving double kink nucleation and propagation. This model gives for the temperature-dependent Peierls stress

$$\tau_P = \frac{\tau_0}{\beta E^{\mathrm{kink}}} \operatorname{arcsinh}\left(\frac{\dot{\gamma}}{\dot{\gamma}_0^{\mathrm{kink}}} e^{\beta E^{\mathrm{kink}}} \right), \tag{1}$$

where β is $1/k_B T$, with k_B being Boltzmann's constant and T the absolute temperature, E^{kink} is the kink energy,[28] τ_0 is the effective Peierls stress, and $\dot{\gamma}_0^{\mathrm{kink}}$ is the reference strain rate. Here, the effective Peierls stress is

$$\tau_0 = \frac{E^{\mathrm{kink}}}{b L^{\mathrm{kink}} l_P} \tag{2}$$

and the reference strain rate is

$$\dot{\gamma}_0^{\mathrm{kink}} = 2 b \rho l_P \nu_D, \tag{3}$$

where b is the Burgers vector, L^{kink} is the kink length, ρ is the dislocation density, ν_D is the attempt frequency which may be identified with the Debye frequency to a first approximation,[24,25] and l_P is the distance between two consecutive Peierls valleys. Physically, E^{kink} is the minimum energy to form a double kink, L^{kink} is the minimum length

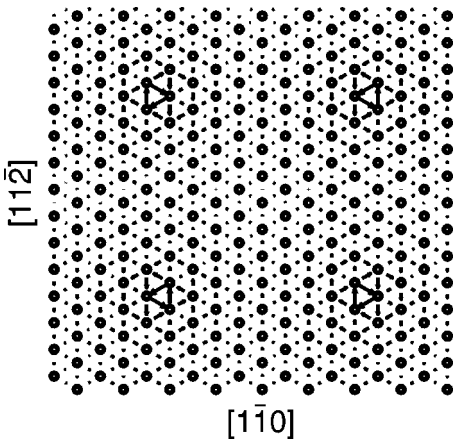

FIG. 3. Quadrupolar unit cell of size 42 Å × 41 Å : relative displacements of neighboring columns of atoms (arrows) and dislocation centers (triad of arrows). Note, that in the calculations half the amount of such cells are used, which can always be done with an appropriate choice of lattice vectors (Ref. 36).

for this double kink, and τ_o is the stress, whose work to move a dislocation a distance l_P is equal to E^{kink}.

Figure 2 shows the fit of Eq. (1) to our atomistic data. To mimic how zero-temperature lattice resistances are generally extracted, we adjust the three unknown parameters (τ_0, E^{kink}, and $\dot{\gamma}_0^{\text{kink}}$)to fit our higher-temperature data *only*. Intriguingly, extrapolation of our higher-temperature results to zero temperature leads to an underestimation of the Peierls stress of between 10% and 20%. We would also expect that a fit to data from a cell sufficiently large to allow for double kink formation (which are only active at nonzero temperatures) would lead to an even larger underestimation of the zero-temperature stress. These results therefore suggest that the general discrepancy between extrapolated experimental values and the calculated values for the zero-temperature Peierls stress may be the result of failure of nonzero-temperature models to properly describe the low-temperature regime. However, since this discrepancy is over a factor of 2, when employing empirical potentials, further calculations would clearly be needed to determine if the underestimation due to extrapolations, when double kinks are capable of forming, could fully account for the discrepancy.

IV. ACCURATE PEIERLS STRESS CALCULATIONS IN SMALL PERIODIC CELLS

Having underscored the need for first-principles electronic-structure studies and already having determined that the most effective boundary conditions for such studies is periodic, we now focus on determining minimal cell size appropriate to calculation of the zero-temperature Peierls stress for a $\langle 111 \rangle$ screw dislocation in a bcc metal when the maximum resolved shear stress is along a $\{110\}$ plane.

To minimize image effects, we employ periodic boundary conditions with a quadrupolar unit cell. Figure 3 shows a differential displacement map[2] of such a cell of size 42 Å × 41 Å in the plane perpendicular to the Burgers vector. In such a map, the dots indicate columns of atoms along the $[111]$, and the vectors between the columns of atoms indicate the relative shift along the Burgers vector due to the presence of a dislocation between each pair of columns, with the vectors scaled so that a vector of full length between the columns corresponds to one-third the Burgers vector. In this ground-state structure of the dislocation, triads of full length vectors surround the center of each dislocation, corresponding to a new displacement by a full Burgers vector upon completion of a closed loop about each center. In the figure, four dislocations are present.

In practice, because of symmetry, the quadrupole cell may be reduced to half the size, when lattice vectors are properly chosen.[36] Since such a reduction is computationally efficient, we now use such smaller cells. Although the computational cells will now only contain two dislocations, we still refer to it as a quadrupolar cell, in order to differentiate it from the dipolar cell, which also has two dislocations but whose periodic images differ.

As Sec. II notes, for calculations of static properties such as the ground-state dislocation core structure, the strain fields from the surrounding dislocations in a quadrupolar array essentially cancel at each dislocation core. However, in a dynamical problem such as the calculation of the Peierls stress, the dislocations begin to interact with the stress fields of the others as they begin to move. Our previous work[4] shows that, for the particular geometry considered here, accurate values for the Peierls stress can be extracted from quite small unit cells provided the proper procedure is followed. We now outline that procedure while reviewing the relevant background.

A. Calculation of Peierls stress within periodic boundary conditions

To calculate the Peierls stress in a small periodic cell, we begin with lattice vectors appropriate to bulk material in the absence of dislocations and then, while relaxing the internal coordinates of the cell, apply increasingly pure ϵ_{xz} strains (using the same Cartesian coordinates as those in Sec. II C) until the dislocations move. Such a strain drives the dislocation along the $[11\bar{2}]$ direction.[28] Before the dislocation moves, the strain energy of the cell increases quadratically,

$$E = \frac{1}{2} C' \epsilon_{xz}^2, \tag{4}$$

where C' is an elastic constant associated with the quadrupole unit cell which can be extracted simply from the energies of the cell as the strain increases. The stress associated with this strain is

$$\sigma_{xz} = C' \epsilon_{xz}, \tag{5}$$

so that at the strain at which the dislocation moves, Eq. (5) gives the Peierls stress.

The great benefit of the above procedure is that it requires a *minimal* search through phase space in order to calculate the Peierls stress and accounts accurately for the effects of the dislocation-dislocation interactions. The C' elastic constant, which is a direct byproduct of the procedure and requires no further calculations, suffices to account accurately

for the main effects of having a cell with a densely packed array of dislocations.[4] This correction prevents most of the effects from working with small unit cells and can differ from that of an equivalent bulk cell by a value of 2 or more.

The above procedure involves several approximations requiring justification. First, we apply strain relative to the lattice vectors of the bulk cell in the absence of the dislocation, rather than those of the quadrupole array. Previously, we have shown through explicit calculation on model interatomic potentials that working with the relaxed lattice vectors of the quadrupolar array does not improve the value calculated for the Peierls stress and therefore is not needed.[4] The reason for this is that although working with the bulk lattice vectors generates artificial stresses, these are primarily diagonal (σ_{ii}), because the greatest effect of the presence of the dislocations is dilation of the system.[4] In the present geometry, such diagonal stresses result only in a constant shift in the energy over the range of applied strain and do not generate driving (Peach-Kohler[28]) forces on the dislocations.

Some slight care must be taken with the above argument. Duesbery and others[3,14] have pointed out that stresses which do not result in driving forces on a dislocation still may affect the overall value of the Peierls stress needed to drive the dislocation, because such stresses may modify the dislocation core structure,[41] an effect not accounted for in linear elasticity theory. This effect of nondriving stresses is, in fact, one of the common violations of the Schmid law that bcc metals exhibit. Diagonal stresses, however, do not have a large effect[3] on the value for the Peierls stress, since they tend to only compress or expand the core. Fortunately, because the bulk lattice vectors should be relatively close to that of the dislocation cell, we expect all of these effects to be quite small, as we have found previously[4] and again verify in the test calculations below.

The second simplification in our procedure is that rather than applying a strain which imposes a pure σ_{xz} stress, we apply a pure ϵ_{xz} strain, which also generates a residual σ_{xy} stress.[28] To generate a pure stress of the form σ_{xz}, one would have to apply an additional ϵ_{xy} strain of a magnitude determined by yet another elastic constant of the quadrupolar array. Because the calculation of this constant would significantly increase the number of calculations required and because the residual σ_{xy} stress[28] acts on the plane perpendicular to the dislocation, and thus does not create a driving force on the dislocations, we simply apply the pure ϵ_{xz} strain. As with the diagonal stress components, although the residual in-plane σ_{xy} stress does not drive the dislocations, it can affect the Peierls stress by modifying the core structure. Unlike the diagonal stress components, the in-plane stress significantly affects the Peierls stress in bcc metals.[3,14] This effect, however, will be small as long as the residual σ_{xy} stress is small compared to the driving σ_{xz} stress. The ratio σ_{xy}/σ_{xz}, is equal to C''/C', where C' is the elastic constant appearing in Eq. (4) and C'' is another combination of elastic constants. In pure bulk cubic materials these constants have the form[28]

$$C' = \frac{1}{3}(C_{11} + C_{44} - C_{12}),$$

$$C'' = -\frac{\sqrt{2}}{6}(2C_{44} + C_{12} - C_{11}),$$

where C_{ij} are the standard elastic constants for cubic materials.

As evidence of the correlation between the ratio of these constants and the errors in the Peierls stress, we note that in our previous study[4] with the same empirical potential as that in Sec. III, the ratio C''/C' varied from approximately 1/5 in the smallest cell studied to less than 1/10 for all other cells, while the error in extracting the Peierls stress went from 18% to less than 2%, respectively. For the potential used in that study, the value of C''/C' computed from bulk elastic constants is 1/90. Since the bulk value of C''/C' within density-functional theory is less than 1/100,[19] we expect the errors in our *ab initio* value of the Peierls stress to be even somewhat smaller. Lending further support to this view is the result of Duesbery and Vitek[41] that demonstrated that the effect of σ_{xy} stresses on core structure is much less for the nondegenerate core structure, which we have in our density-functional calculations, than for the degenerate core structures, which we had in our interatomic potential calculations.[4]

B. Demonstration

To demonstrate the efficacy of the above procedure, we now proceed to extract the Peierls stress in the $\langle 112 \rangle$ direction for vanadium and tantalum from calculations in small periodic cells, when the maximum resolved shear stress is along a {110} plane. In all calculations we calculate the Peierls stress for an infinite straight dislocation, since our periodic cells have the lattice vector $\vec{a}_3 = a[111]/2$ along the dislocation line. To allow comparison with the Peierls stress of isolated dislocations, we employ empirical potentials for this demonstration. For vanadium we use the Finnis-Sinclair[42] potential with modifications made Ackland and Thetford,[43] and for tantalum we use the same potential as that used in Sec. III but with a slight adjustment of parameters to produce a nondegenerate core structure. The bulk ratios for C''/C' for vanadium and tantalum within these models are 1/10 and 1/6.5, respectively, much larger than the density-functional theory value.

To determine the reference value for the Peierls stress, we employed cylindrical boundary conditions with large amounts of material, increasing the radii of the cylinders until the boundary forces were small[17] and the Peierls stress approached an asymptotic value. To extract the Peierls stress from within periodic boundary conditions, we follow precisely the procedure that Sec. IV A outlines.

Figure 4 shows the resulting energy versus strain curve for vanadium within a periodic cell of size 42 Å $\times$ 20 Å . At a strain ≈ 0.054, the curve exhibits a discontinuity, signaling the critical strain for moving the dislocation. The curvature of the fit determines the elastic constant C' through Eq. (4). Finally, combining this value of C' with the observed critical strain, Eq. (5), yields the Peierls stress. We repeated this procedure for tantalum as well.

Table II summarizes our results for both vanadium and tantalum. The table shows that the errors are relatively small,

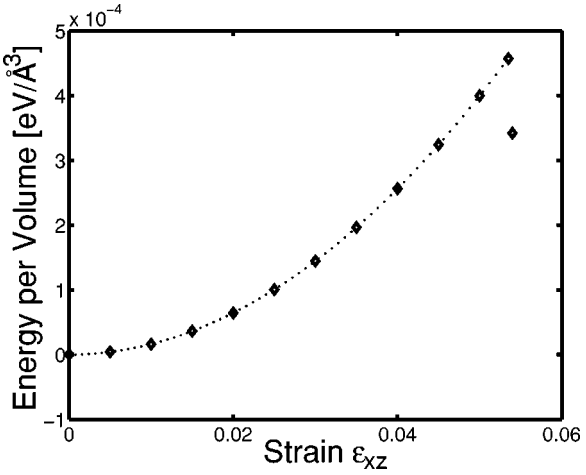

FIG. 4. Energy versus strain of vanadium in a quadrupolar cell of size 42 Å × 20 Å . Diamonds denote the energy calculated at various strains. The dotted line is a quadratic fit up to the Peierls stress.

much smaller than the general discrepancy between empirical potentials and the experimental extrapolations. It is also noteworthy that the potentials employed in this demonstration exhibit C''/C' ratios over an order-of-magnitude larger than those of density-functional theory. From these and previous results,[4] we conservatively estimate that the error in the Peierls stress in the density-functional calculations below should be no greater than $\approx 20\%$.

V. DENSITY-FUNCTIONAL RESULTS AND DISCUSSION

A. Computational details

All of our first principles electronic-structure calculations employ the plane-wave density-functional theory (DFT) pseudopotential approach[32] within the local-density approximation.[44,45] We employ a pseudopotential of the Kleinman-Bylander form[46] with s, p, and d nonlocal channels that have been successfully used in previous works[19,47] and a plane-wave basis with cutoff of 40 Ry. As justified above, we employ a quadrupolar supercell, containing two dislocations, of sizes $\vec{r}_1 = 5a[1,\bar{1},0]$, $\vec{r}_2 = (3/2)a[1,1,\bar{2}]$, and $\vec{r}_3 = a[1,1,1]/2$, where $a = 3.25$ Å is the lattice constant of the cubic unit cell. The lattice vectors of this cell are $\vec{a}_1 = \vec{r}_1/2 - \vec{r}_2 + \vec{r}_3/2$, $\vec{a}_2 = \vec{r}_1/2 + \vec{r}_2 + \vec{r}_3/2$, and $\vec{a}_3 = \vec{r}_3$. To carry out the integrations over the Brillouin zone we use a nonzero electronic temperature of $k_B T = 0.1$ eV to facilitate integration over the Fermi surface and sample the zone at sixteen special k points.[48] These choices give energy differences reliably to within 0.1 eV/atom. Finally, to determine the electronic structure, we minimize using the analytically continued functional approach,[49] expressed within the DFT++ (Ref. 50) formalism.

TABLE II. Magnitude of percentage of error in calculating the Peierls stress in periodic cells of two different sizes from empirical potentials for vanadium and tantalum.

	23 Å×11.5 Å	42 Å×20 Å
Ta	25%	10%
V	26%	11%

B. Energy landscapes

To demonstrate the discrepancies that occur between the predictions of empirical potentials and first-principles electronic-structure studies, we compare the energy landscape for a dislocation moving along a reaction coordinate from the easy-core configuration to the hard-core configuration[2,10] for both molybdenum and tantalum as determined within MGPT (Ref. 12) and as calculated using *ab initio* studies. Within MGPT, we carried out the calculation for molybdenum ourselves and used the hard-easy-core energy difference reported in the literature[11] for tantalum. Within density-functional theory, we have calculated the energy at a number of points along the reaction pathway for tantalum, and for molybdenum we report the difference between the easy-core and hard-core configurations as found in Ref. 19. We also note that, for molybdenum, within density-functional theory, the hard-core configuration was not stable and therefore the stable structure found within MGPT was used as the reference state.

Figure 5 shows the results. Most noticeably, the atomistic landscapes are three times stiffer than the *ab initio* landscapes. This raises the question of whether the approximate factor-of-3 overestimate of theoretical calculations over the extrapolation of the experimental Peierls stresses to zero temperature is due to defects in the interatomic potentials or to failures in the connection between the experiments and the theoretical calculations.

C. Verification of cell size

To compute the Peierls stress, we employ a cell of dimensions 23 Å × 12 Å . To verify that long-range electronic-structure effects in metals do not interfere with results in such a cell, we compare the core structure reported previously[19] for this cell with a new calculation using a larger cell. Figure 6 shows the result for the core structure in a cell of size 41 Å × 20 Å . The quadrupole supercell has sizes $\vec{r}_1 = 9a[1,\bar{1},0]$, $\vec{r}_2 = (5/2)a[1,1,\bar{2}]$, and $\vec{r}_3 = a[1,1,1]/2$. The lattice vectors are similarly $\vec{a}_1 = \vec{r}_1/2 - \vec{r}_2 + \vec{r}_3/2$, $\vec{a}_2 = \vec{r}_1/2 + \vec{r}_2 + \vec{r}_3/2$, and $\vec{a}_3 = \vec{r}_3$. Here we use eight special k points,[51] which is sufficient since the lattice vectors in the plane of the dislocation have doubled.

We note that the core structure is very similar to previous studies[19] which used a smaller cell equal in size to the one we employ for our calculation of the Peierls stress. We therefore do not expect the long-range nature of electronic effects in metallic systems to greatly affect the value which shall extract for the Peierls stress. We also note that the empirical potential results for tantalum (Sec. IV) had a very large cutoff of 9 Å and accurate results were obtained in the smallest cells used in those calculations. These facts lend confidence to the reliability of our density-functional theory predictions below.

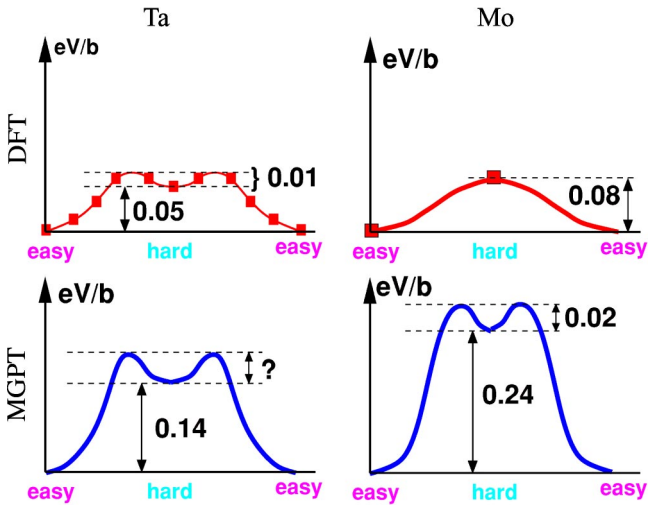

FIG. 5. (Color online) Energy landscape per Burgers vector along a reaction coordinate when going from the easy-core to the hard-core configurations in tantalum and molybdenum: density-functional theory (squares in upper panels) and MGPT (curves in lower panels). *Ab initio* results for molybdenum are from Ref. 19, and the MGPT results for tantalum are from Ref. 11.

D. Results for the Peierls stress

Figure 7 shows our density-functional theory results for energy as a function of strain following the procedure of Sec. IV A. We regard each data point as fully relaxed when the magnitude of the residual force on each atom is less than 0.005 eV/Å .

From Fig. 7 it is apparent that, at a strain of 0.05, the Peierls stress has been exceeded, whereas at a strain of 0.04, the energy curve lies on the elastic solution. From the curvature of the data in the elastic region ($C'=35.2$ GPa) and with these critical strains, we bound the Peierls stress (σ_{xz}) to be between 1.41 GPa and 1.76 GPa. These results are slightly lower than the previous density-functional results of ≈ 1.8 GPa obtained using Greens-function boundary conditions.[8] However, both results are still in reasonable agreement, as we expect our results to be within 20% of the infinite cell limit, while it is unclear how the domain boundary affected the value of the Peierls stress in the Greens-function boundary condition calculation.

Figures 8 and 9 show differential displacement maps[2] of the dislocation configuration at strains of 0.04 and 0.05, respectively. The solid upright triangles in the figures represent the locations of the center of the dislocations before the application of strain and the upsidedown, triangles represent the center of the dislocations once they have moved. Figure 8 shows the relaxed dislocation core to remain in the position of its unstressed state, whereas Fig. 9 shows that at an applied strain of 0.05, the dislocation moves onto the next triad of columns of atoms. This glide is consistent with such screw dislocations since the initial displacement is along the $(01\bar{1})$ plane. The subsequent motion should be along the $(1\bar{1}0)$ plane, since the core symmetry is broken prior and upon motion,[14] and hence overall motion is along a {112} plane (twinning direction), consistent with the previous density-functional theory[8] calculations.

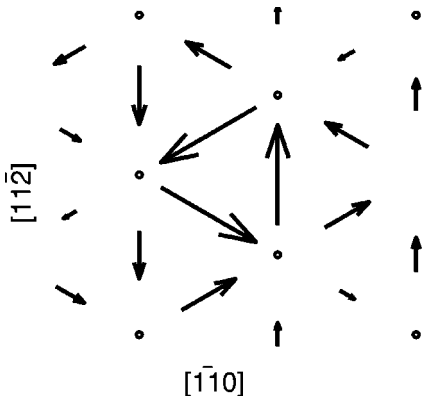

FIG. 6. Easy-core structure for tantalum calculated within density- functional theory. This cell of size 41 Å × 20 Å gives very similar results to the cell of size 23 Å × 12 Å , used in Ref. 19.

Intriguingly, despite the fact that the *ab initio* energy landscape is *less* corrugated than that of the interatomic potential by a factor of nearly 3 (Fig. 5), the above *ab initio* result for the Peierls stress is over a factor-of-2 *larger* than the empirical potential result (Table I). Moreover, our result is over a factor-of-5 *larger* than extrapolations of experimental data to zero temperature,[15] a discrepancy much larger than any effects from the use of either our relatively small quadrupolar cell or the local-density approximation to density-functional theory. Certainly, as Sec. III shows, some of this discrepancy can be due to the extrapolation of experimental data to zero temperature. However, errors in the zero-temperature extrapolation may not likely account for all of the discrepancy since the underestimation in Fig. 2 is only $\approx 10\%-20\%$. Although we made the conjecture that double kink formation may even make these errors larger, we would not expect this effect to account for the 500% difference between the *ab initio* results and the experimental findings. One must therefore consider the possibility of other factors such as the ef-

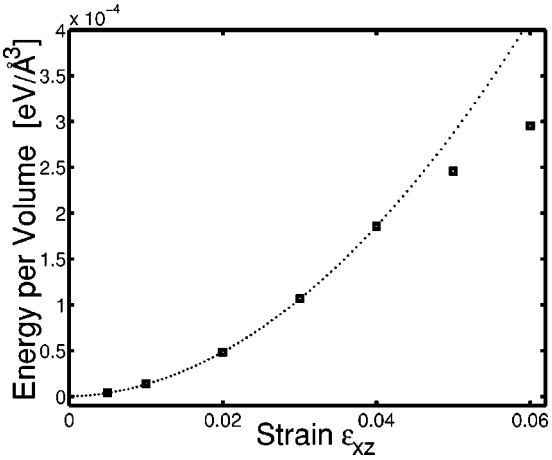

FIG. 7. Energy versus strain for tantalum in a cell of size 23 Å × 12 Å , calculated within density-functional theory. Squares denote the calculate energy at various strains. The line is a quadratic fit to the first five data points. The graph indicates that the points with strain at and above 0.05 ($\sigma_{xz}=1.76$ GPa) will be at a stress above the Peierls stress.

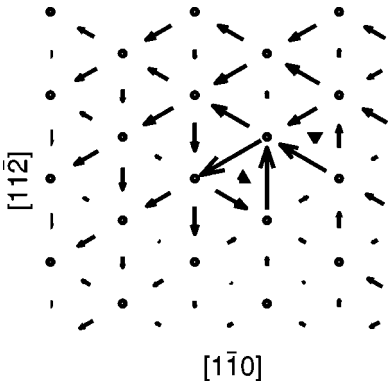

FIG. 8. Differential displacement map at an applied strain of 0.04 ($\sigma_{xz}=1.41$ GPa). The cell has converged to within the tolerance defined in the text. The solid upright triangle is the location of the center of the dislocation, under no stress. The center of the dislocation, at this applied stress, has not moved.

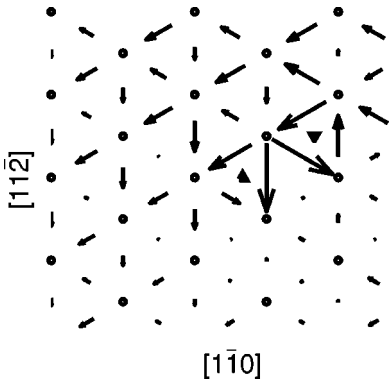

FIG. 9. Differential displacement map at an applied strain of 0.05 ($\sigma_{xz}=1.76$ GPa). The cell has converged to within the tolerance defined in the text. This figure shows that the core has moved from the old triad (solid upright triangle) to a new triad (upside-down triangle) along a $\langle 112 \rangle$ direction.

fects of junctions,[52] defects, surfaces, strain-rate dependencies, curved dislocations, screening from the presence of other dislocations, or a combination of effects to accurately predict the experimental results.

VI. CONCLUSION

This work explores various aspects of the Peierls stress for the $\langle 111 \rangle$ screw dislocation in bcc tantalum. The first nonzero-temperature results for the Peierls stress in this system show both a strong orientation- and temperature-dependent response, consistent with experimental results. These data also demonstrate that common extrapolations of experimental data tend to underestimate the zero-temperature limit.

We have also presented a density-functional theory calculation for the Peierls stress within periodic boundary conditions, the approach best suited to metallic systems. The value we find for the Peierls stress is substantially larger than both the experimental extrapolations and current empirical potential results. This difference is much larger than errors which could normally be attributed to the use of a relatively small unit cell or the local-density approximation to density-functional theory. The error is also significantly larger than the underestimation we have seen in the the extrapolation of nonzero-temperature data to zero temperature, thus supporting the notion that mechanisms other than the simple Peierls resistance may play an important role in controlling the process of low-temperature slip.

ACKNOWLEDGMENTS

The authors would like to thank Guofeng Wang for providing us with the parameters for the qEAM potential. This work was supported by an ASCI ASAP Level 2 grant (Contract Nos. B338297 and B347887). Computational support on ASCI Blue Pacific was provided through the Cal-Tech DOE ASCI center. We thank the members of the H division at Lawrence Livermore National Laboratories for providing the Ta pseudopotential, the Mo MGPT code, and many useful discussions.

*Current address: Department of Applied Physics, California Institute of Technology, Pasadena, California 91125.
†Current address: Theoretical Division, Los Alamos National Laboratory, Los Alamos, New Mexico 87545.

[1] M.S. Duesbery, *Dislocations 1984* (CNRS, Paris, 1984), p. 131.
[2] V. Vitek, Cryst. Lattice Defects **5**, 1 (1974), *and references therein*.
[3] M.S. Duesbery, Proc. R. Soc. London, Ser. A **54**, 145 (1984).
[4] D.S. Segall, T.A. Arias, A. Strachan, and W.A. Goddard III, J. Comput.-Aided Mater. Des. **8**, 161 (2001).
[5] G. Wang, A. Strachan, T. Cagin, and W.A. Goddard III, Mater. Sci. Eng., A **309**, 133 (2001).
[6] S. Rao and C. Woodward, Philos. Mag. A **81**, 1317 (2001).
[7] C. Woodward and S. Rao, Philos. Mag. A **81**, 1305 (2001).
[8] C. Woodward and S. I. Rao, Phys. Rev. Lett. **88**, 216402 (2002).
[9] L.H. Yang, P. Soderlind, and J.A. Moriarty, Philos. Mag. A **81**, 1355 (2001).
[10] W. Xu and J.A. Moriarty, Comput. Mater. Sci. **9**, 348 (1998).
[11] J.A. Moriarty, W. Xu, P. Soderlind, J. Belak, L.H. Yang, and J. Zhu, J. Eng. Mater. Technol. **121**, 120 (1999).
[12] W. Xu and J.A. Moriarty, Phys. Rev. B **54**, 6941 (1996).
[13] S. Takeuchi, in *Interatomic Potentials and Crystalline Defects*, Lee [American Institute of Mechanical Engineers (AIME) New York, 1980], p. 201.
[14] K. Ito and V. Vitek, Philos. Mag. A **81**, 1387 (2001).
[15] M. Tang, L.P. Kubin, and G.R. Canova, Acta Mater. **46**, 3221 (1998).
[16] W. Sigle, Philos. Mag. A **79**, 1009 (1999).
[17] V.J. Shenoy and R. Phillips, Philos. Mag. A **76**, 367 (1997).
[18] V.V. Bulatov, O. Richmond, and M.V. Glasov, Acta Mater. **47**, 3507 (1999).
[19] Sohrab Ismail-Beigi and T.A. Arias, Phys. Rev. Lett. **84**, 1499 (2000).
[20] T.E. Mitchell, R.A. Foxall, and P.B. Hirsch, Philos. Mag. **8**, 1895 (1963).
[21] H. Suzuki, *Dislocation Dynamics* (McGraw-Hill, New York,

1968), p. 679.
[22] K. Kimura, S. Takeuchi, and K. Masuda-Jindo, Philos. Mag. A **60**, 667 (1988).
[23] U.F. Kocks, A.S. Argon, and M.F. Ashby, *Thermodynamics and Kinetics of Slip*, in *Progress in Materials Science*, edited by B. Chalmers, J.W. Christian, and T.B. Massalshi (Pergamon, New York, 1975), Vol. 19.
[24] A.M. Cuitino, L. Stainier, G. Wang, A. Strachan, T. Cagin, W.A. Goddard III, and M. Ortiz, J. Comput.-Aided Mater. Des. **8**, 127 (2001).
[25] L. Stainier, A.M. Cuitino, and M. Ortiz, J. Mech. Phys. Solids **50**, 1511 (2002).
[26] J.E. Sinclair, J. Appl. Phys. **42**, 647 (1971).
[27] S. Rao, C. Hernandez, J. Simmons, T. Parthasarathy, and C. Woodward, Philos. Mag. A **77**, 231 (1998).
[28] J. P. Hirth and J. Lothe, *Theory of Dislocations*, 2nd ed. (Wiley, New York, 1982).
[29] A.N. Stroh, Philos. Mag. **3**, 625 (1958).
[30] A.K. Head, Phys. Status Solidi **6**, 461 (1964).
[31] Sohrab Ismail-Beigi and T.A. Arias, Phys. Rev. Lett. **82**, 2127 (1999).
[32] M.C. Payne, M.P. Teter, D.C. Allen, T.A. Arias, and J.D. Joannopoulos, Rev. Mod. Phys. **64**, 1045 (1992).
[33] S. Marklund, Phys. Status Solidi B **85**, 673 (1978).
[34] T.A. Arias and J.D. Joannopoulos, Phys. Rev. Lett. **73**, 680 (1994).
[35] N. Lehto and S. Oberg, Phys. Rev. Lett. **80**, 5568 (1998).
[36] J.R.K. Bigger, D.A. McInnes, A.P. Sutton, M.C. Payne, I. Stich, R.D. King-Smith, D.M. Bird, and L.J. Clarke, Phys. Rev. Lett. **69**, 2224 (1992).
[37] A. Strachan, T. Cagin, O. Gulseren, S. Mukherjee, R.E. Cohen, and W.A. Goddard III, cond-mat/0208027 (unpublished).
[38] M. Parinello and A. Rahman, J. Appl. Phys. **52**, 7182 (1981).
[39] W.G. Hoover, Phys. Rev. A **31**, 1695 (1985).
[40] W. Wasserbach, Philos. Mag. A **53**, 335 (1986).
[41] M.S. Duesbery and V. Vitek, Acta Mater. **46**, 1481 (1998).
[42] M.W. Finnis and J.E. Sinclair, Philos. Mag. A **50**, 45 (1984).
[43] G.J. Ackland and R. Thetford, Philos. Mag. A **56**, 15 (1987).
[44] D.M. Ceperley and B.J. Alder, Phys. Rev. Lett. **45**, 566 (1980).
[45] J.P. Perdew and A. Zunger, Phys. Rev. B **23**, 5048 (1981).
[46] L. Kleinman and D.M. Bylander, Phys. Rev. Lett. **48**, 1425 (1982).
[47] C. Woodward, S. Kajihara, and L.H. Yang, Phys. Rev. B **57**, 13 459 (1998).
[48] The k-point set is $\pm\frac{1}{32}$({1,1,2}, {17,15,2}, {3,3,6}, {19,-13,6}, {5,5,10}, {21,-11,10}, {7,7,14}, {23,-9,14}). Note that because of symmetry our quadrupole cell has only two dislocations. Without taking advantage of this symmetry the cell would double and have four dislocations with lattice vectors $\vec{b}_1=5a[1,\overline{1},0]$, $\vec{b}_2=3a[1,1,\overline{2}]$, and $\vec{b}_3=a[1,1,1]/2$. The above k points, for the smaller cell, would then map onto eight special k points $k_1=k_2=0$, $k_3\in\pm\{\frac{1}{16}, \frac{3}{16}, \frac{5}{16}, \frac{7}{16}\}$, for the larger cell, where k_1,k_2, and k_3 are generated from the reciprocal lattice of $\{\vec{b}_i\}$.
[49] T.A. Arias, M.C. Payne, and J.D. Joannopoulos, Phys. Rev. Lett. **69**, 1077 (1992).
[50] S. Ismail-Beigi and T.A. Arias, Comput. Phys. Commun. **128**, 1 (2000).
[51] In the larger cell the k-point set is $\pm\frac{1}{32}$({1,1,2}, {3,3,6}, {5,5,10}, {7,7,14}).
[52] V.V. Bulatov and W. Cai, Phys. Rev. Lett. **89**, 115501 (2002).